Electronic Supplementary Material (ESI) for Journal of Materials Chemistry C.

Supplementary Files

Sonochemical functionalization of low-dimensional surface oxide of galinstan for heterostructured optoelectronic applications

Mohammad Karbalaei Akbari, [a,b]* Zhenyin Hai,[a,b] Zihan Wei,[a,b] Ranjith K. Ramachandran,[c] Christophe Detavernier,[c] Malkeshkumar Patel,[d] Joondong Kim,[d] Francis Verpoort,[a,e] Hongliang Lu[f] and Serge Zhuiykov,[a,b]*

[a] Center for Environmental & Energy Research, Ghent University Global Campus, 21985, Incheon, South Korea.

[b] Department of Green Chemistry and Technology, Faculty of Bioscience Engineering, Ghent University, 9000 Ghent, Belgium.

[c] Department of Solid State Science, Ghent University, Krijgslaan 281/S1, 9000 Ghent, Belgium.

[d] Photoelectronic and Energy Device Application Lab, Multidisciplinary Core Institute for Future Energies, Incheon National University, South Korea.

[e] Laboratory of Organometallics, Catalysis and Ordered Materials, State Key Laboratory of Advanced Technology for Materials Synthesis and Processing; Center for Chemical and Material Engineering, Wuhan University of Technology, 430070 Wuhan, P.R. China

[f] School of Microelectronic, Fudan University, Shanghai, P.R. China

* - Corresponding author: serge.zhuiykov@ugent.be; mohammad.akbari@ugent.be

S1: Material Synthesis

Different amounts of $AgNO_3$ and $SeCl_4$ were initially weighted and added to 10 mg of deionized water (DIW) to produce 1 mM, 5 mM and 10 mM of their ionic solutions. Since $SeCl_4$ strongly reacts with moisture of atmosphere (produce corrosive HCl gas) and can also corrode metal, plastic tools in highly dried atmosphere were used to weight $SeCl_4$. Salts were dissolved in solvent even without using any mechanical agitation. However, samples were stirred for 3 min. The Final solutions were ultimately colorless even after several days of rest. Then, accurately weighted (50 mgr) galinstan alloy was dropped into ionic solutions. It was observed that the surface of alloying droplets turned into different colors. In the case of DIW, the surface of galinstan droplet lost its first shinny face (Figure S1), indicating the formation thick surface oxide films.

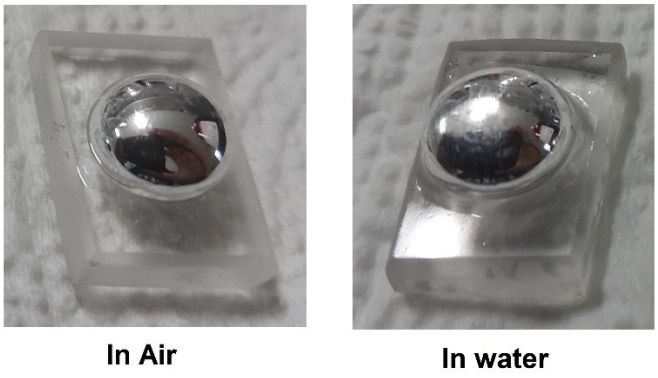

Figure S1. Galinstan droplets in air and after removing DIW from its surface.

In the case of Ag ionic solutions the color of galinstan droplets was greyish and the samples even lost their integrity after 1 h in ionic liquid. It was observed that in high concentration ionic

solutions the dendrite like structures start to nucleate and growth until all of the liquid droplet turned into a black grayish products of branched solids. It is evidently related to the strong galvanic replacement reaction between Ag ions and galinstan. However in the solution with less amount of Ag ions, the shiny color of surface only turned into to light grey after 24 hr. The stop of reaction can be attributed to the full consumption of Ag ions in solution (Figure S2).

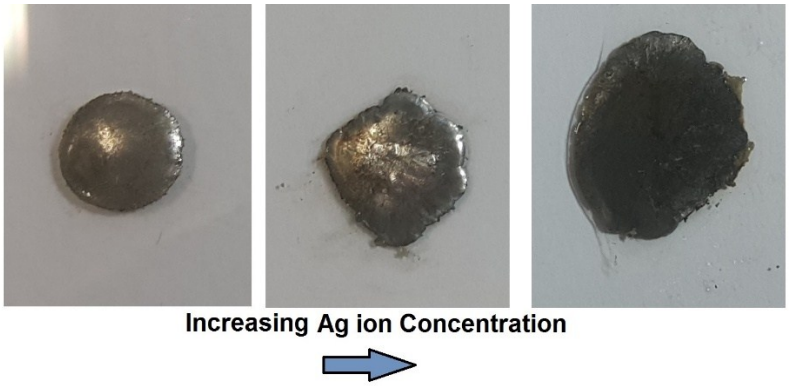

Figure S2. The effect of Ag ion concentration (1 to 10 mM) on galinstan droplets.

Nevertheless, in the case of Se ion containing solutions the reaction was not destructive even at the high concentration of Se ions. It was observed that brow film covered the surface of galinstan droplets which can be related to nucleation of Se or Se rich phases on the surface of alloy.

Figure S3. The effect of Se ion concentration (1 to 10 mM) on surface of galinstan droplets.

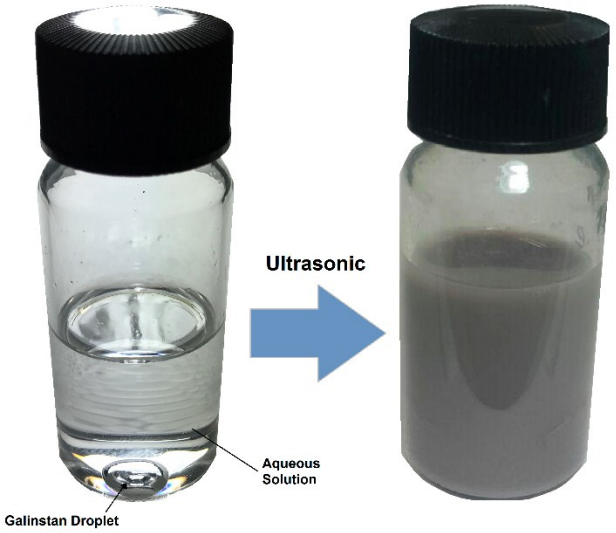

Figure S4. Nanoparticles are distributed in aqueous solution after ultrasonic process.

Figure S5. The slurry over the surface of centrifuged samples, containing Se ions.

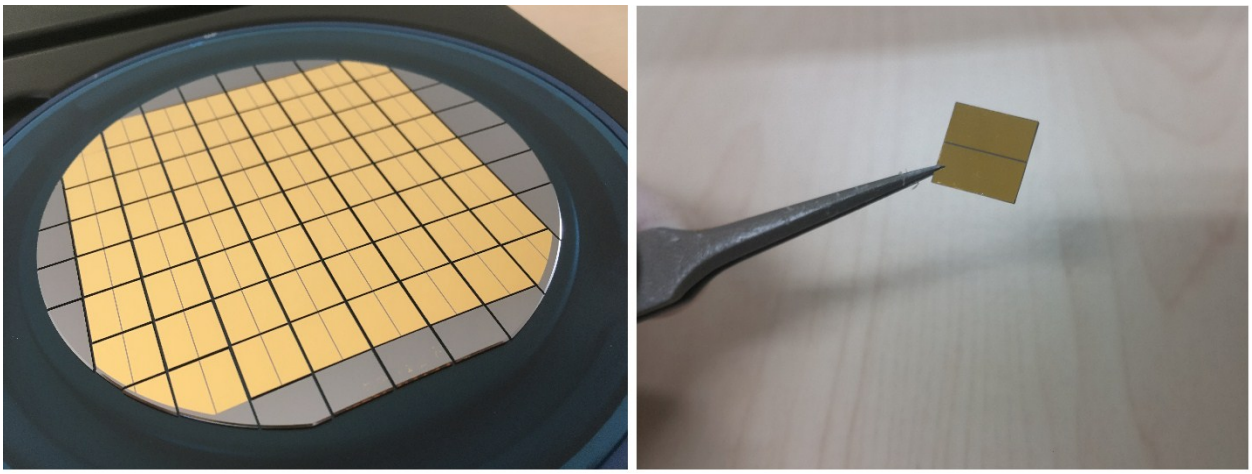

Figure S6. Wafer-scale atomic layer deposition of TiO_2 film over $Au/SiO_2/Si$ electrodes.

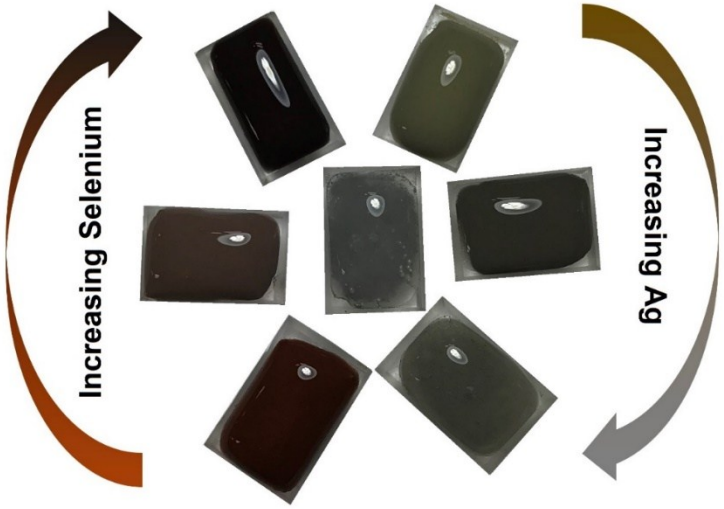

Figure S7. The level of color of nanoparticle suspensions with different Ag and Se concentration (1 to 10 mM) in liquid, the middle sample was synthesized in DIW.

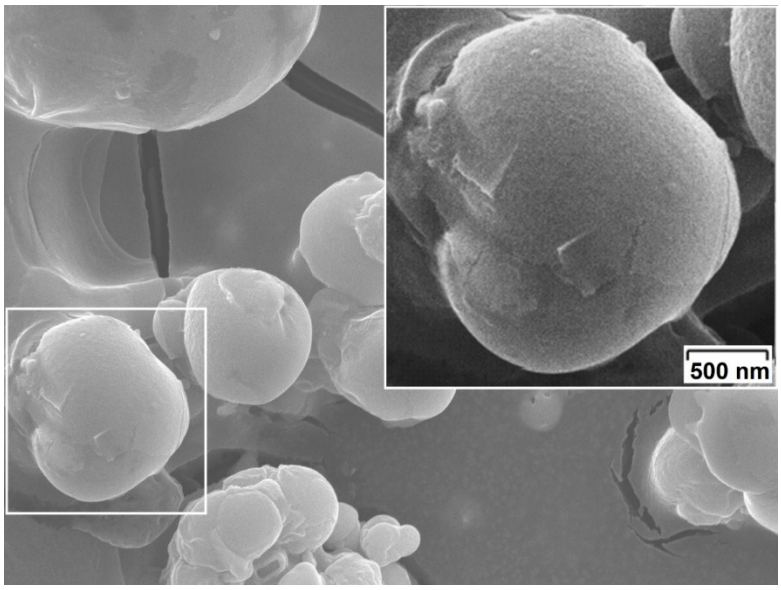

Figure S8. Formation of irregular shaped nanoparticles after ultrasonic assisted synthesis of galinstan nanoparticles. The presence of fractured ultra-thin skin oxide on the surface of nanoparticle is evidently seen. It seems that during the size reduction of nanoparticles in ultrasonic process, brittle skin oxides break and separate from host liquid alloy. Ultrasonic waves will also further assist the separation process.

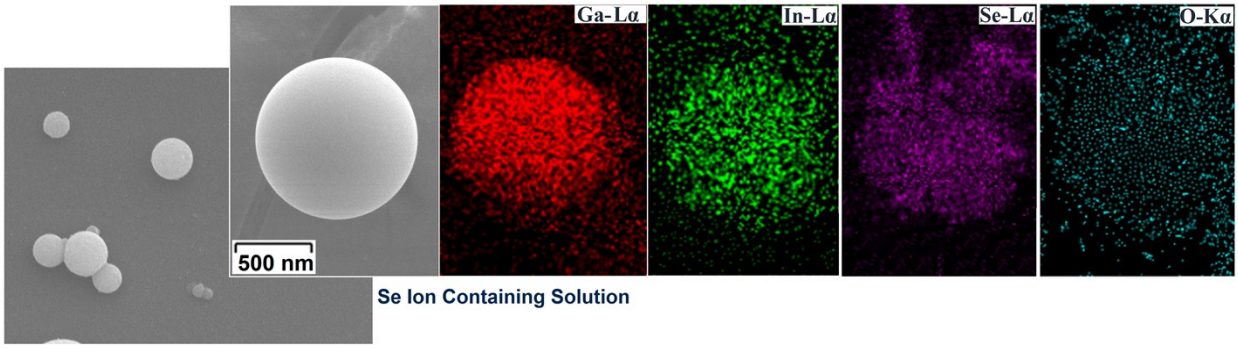

Figure S9. The spherical morphology of nanoparticles and distribution of alloying elements on the surface of galinstan nanoparticles synthesized in Se containing aqueous solution.

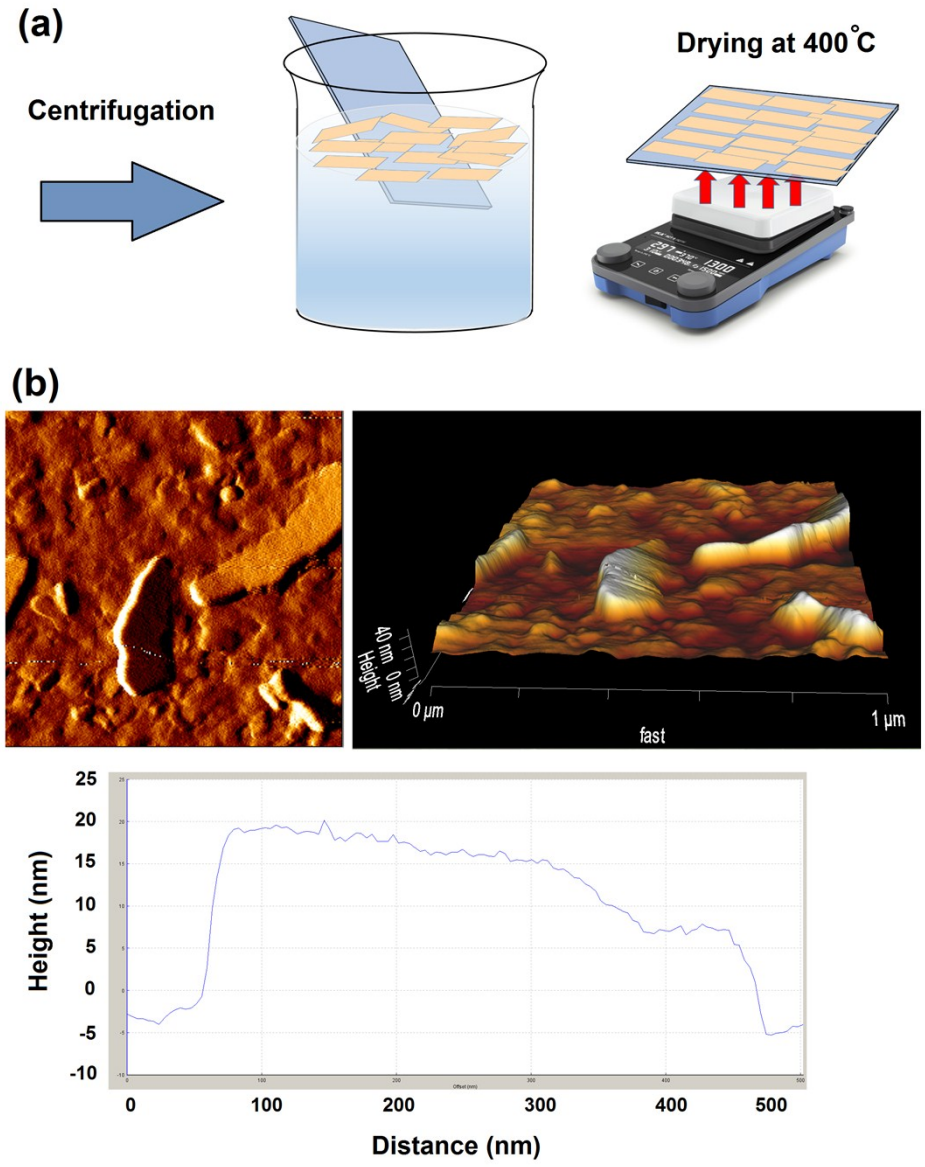

Figure S10. (a) The Schematic of hydrographical printing technique. Nanosheets were separated and then extracted from the liquid suspension by centrifugation. Slurry contains floated nanosheets over the surface of liquid. The extracted nanosheets then were dried overnight by using a hotplate (at 400 ^{0}C) in uncontrolled atmosphere and then again stored in DIW water. The characterization techniques were then performed on extracted nanosheets. Employment of higher temperature drying process of nanosheets were accompanied by agglomeration of them and undesired oxidation of metallic elements (Se and Ag). (b) An atomic force microscope (AFM, JPK NanoWizard) was used to measure the thickness of nanosheets. The thickness profile of an individual extracted Ga_2O_3 nanosheets is demonstrated.

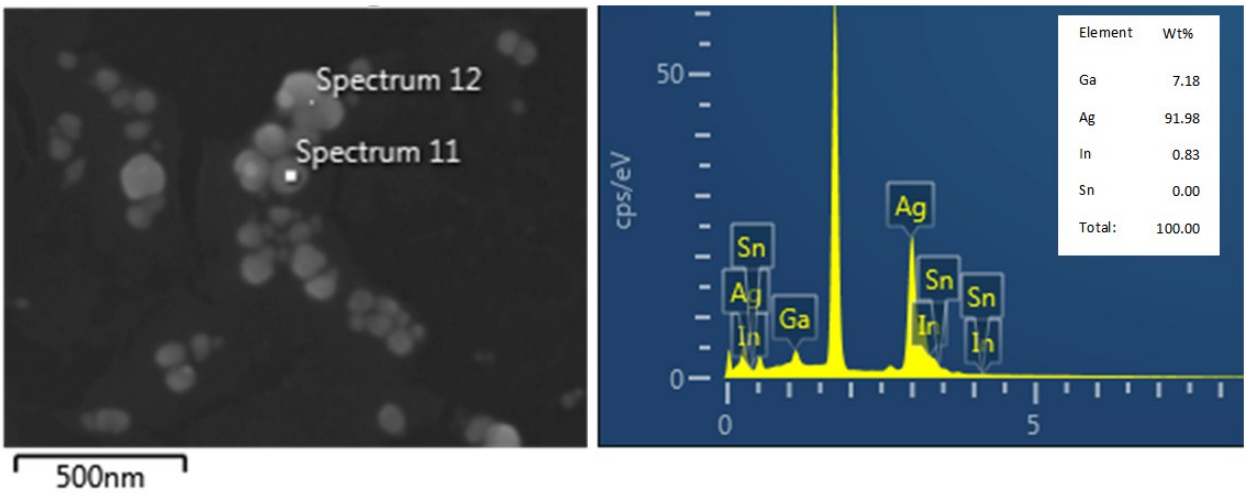

Figure S11. Silver nanoparticles as the by-product of sonochemical technique.

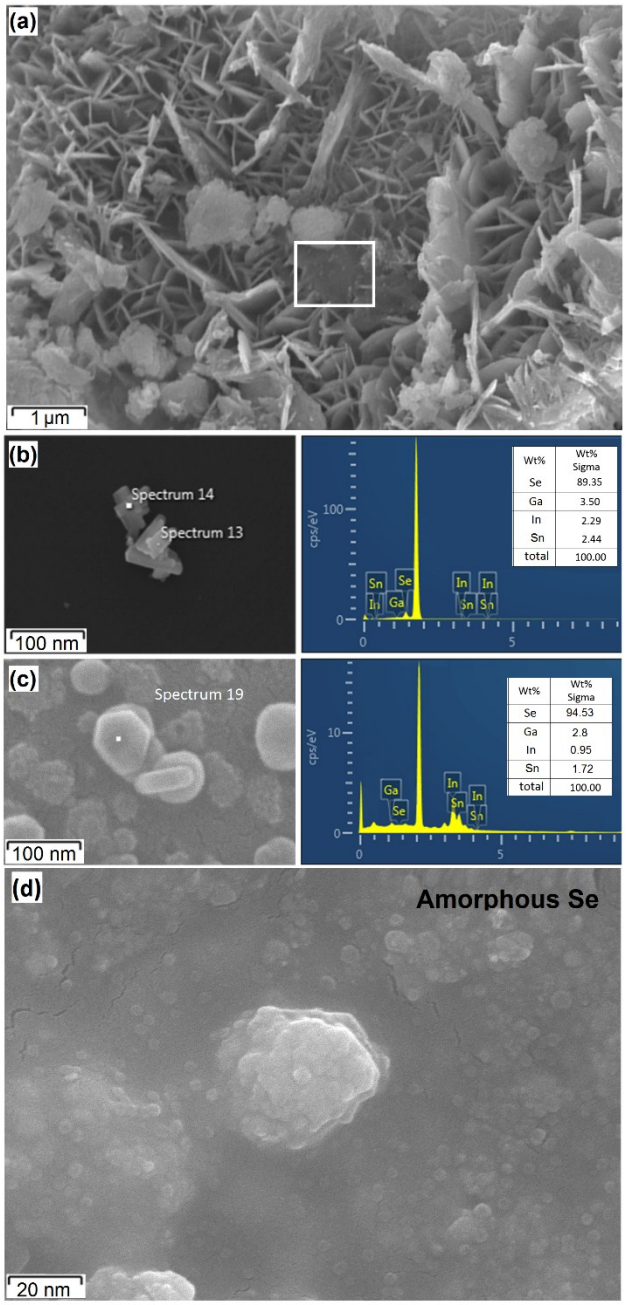

Figure S12. (a) Ga_2O_3 (Se) nanosheets. In (b) and (c) the presence of crystalline and (d) amorphous Se nanostructures are observed.

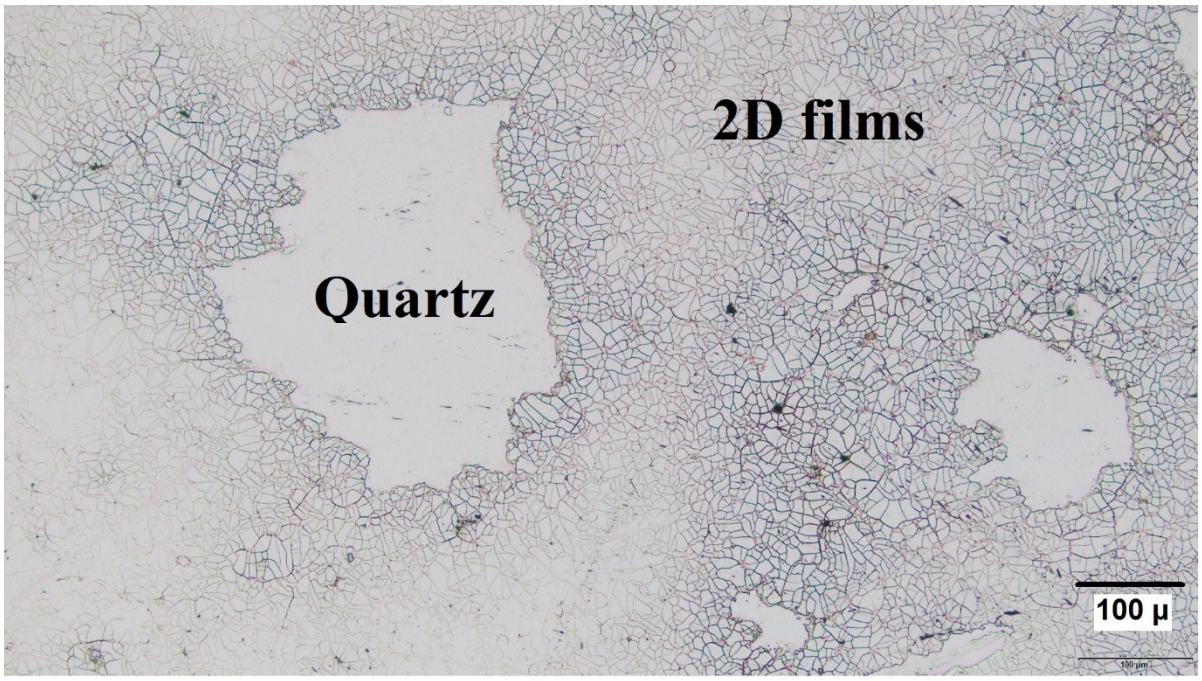

Figure S13. Large-area exfoliation of nanosheets on quartz substrate.

S2-Calculation of Schottky barrier height

Barrier height of a metal–semiconductor contact can be experimentally measured and determined by using I-V curves. Considering that the current is due to thermionic emission, the relation between the applied forward bias and current can be expressed by[1] eq. (1):

$$J = J_0 \exp\left(\frac{qv}{nkt}\right)$$

(1)

Where *n* is ideally factor, T is the temperature in Kelvin, *q* is the electron charge, *k* is the Boltzmann constant and I_0 is the reverse saturation current which can be extracted by extrapolation the straight line of lnI to intercept the axis at zero voltage. The Schottky barrier height (SBH) can be calculated by extrapolation of semi-logarithmic *J-V* curves to V=0. The SBH can be calculated from (2):

$$\emptyset_B = \frac{kT}{q} Ln \frac{T^2 A^*}{J_0}$$

(2)

$$A^* = \frac{4\pi m^* k^2}{h^3}$$

(3)

Where m^* is the effective electron mass, and *h* is the Planck's constant. The A^* is the effective Richardson constant[2,3] which is equal to 41.1 $Acm^{-2}K^{-2}$. The experimental *J-V* characteristics and the logarithmic scale of the same graphs are shown in Figure S14, S15 and S16. We used low forward bias of *J-V* curves to measure the SBH at Au/Ga_2O_3 junctions. Taking the logarithmic version of eq. 1, we can extract the *n* and I_0 from the slop and Y axis of *LnJ-V* plot. After performing least square fitting on the *LnJ-V* plot in the linear region, the values of n and J_0 from the slop and the Y-axis can be determined.

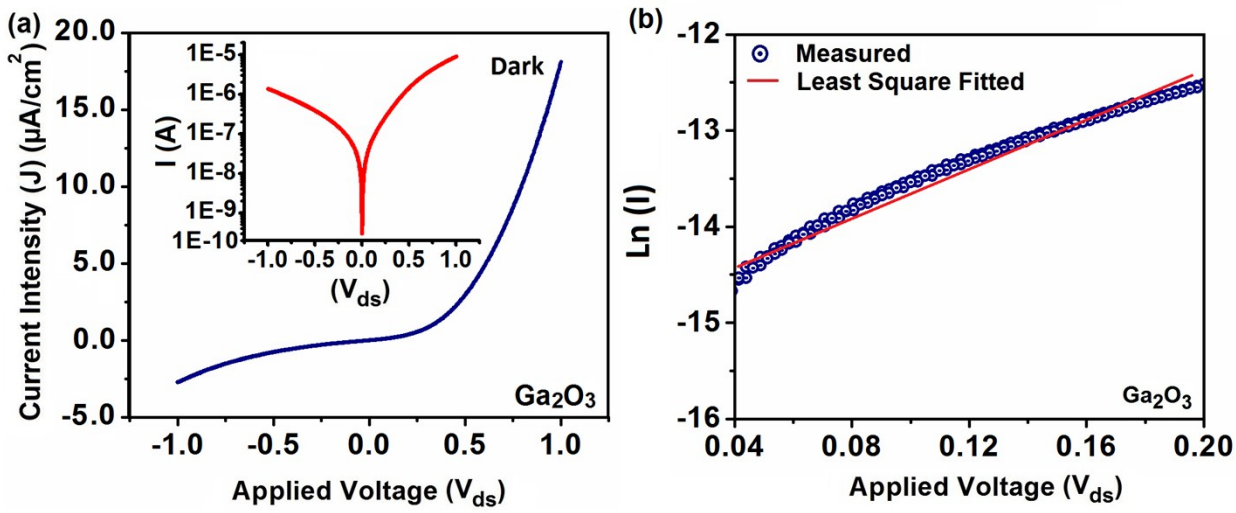

Figure S14. The *J*-V_{ds} characteristics of Ga_2O_3 nanosheets and (b) *LnJ*-*V* plot of the Au/Ga_2O_3 junction (Schottky diode) at the 273K.

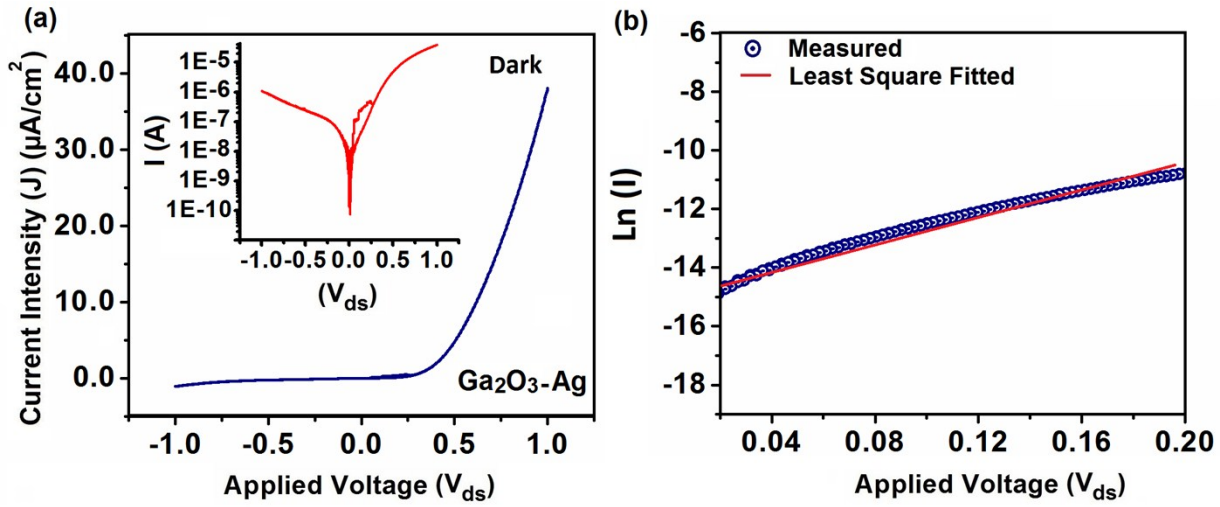

Figure S15. The *J*-V_{ds} characteristics of Au/Ga_2O_3 (Ag) nanosheets device and (b) *LnJ*-*V* plot of the Au/Ga_2O_3 (Ag) junction (Schottky diode) at the 273K.

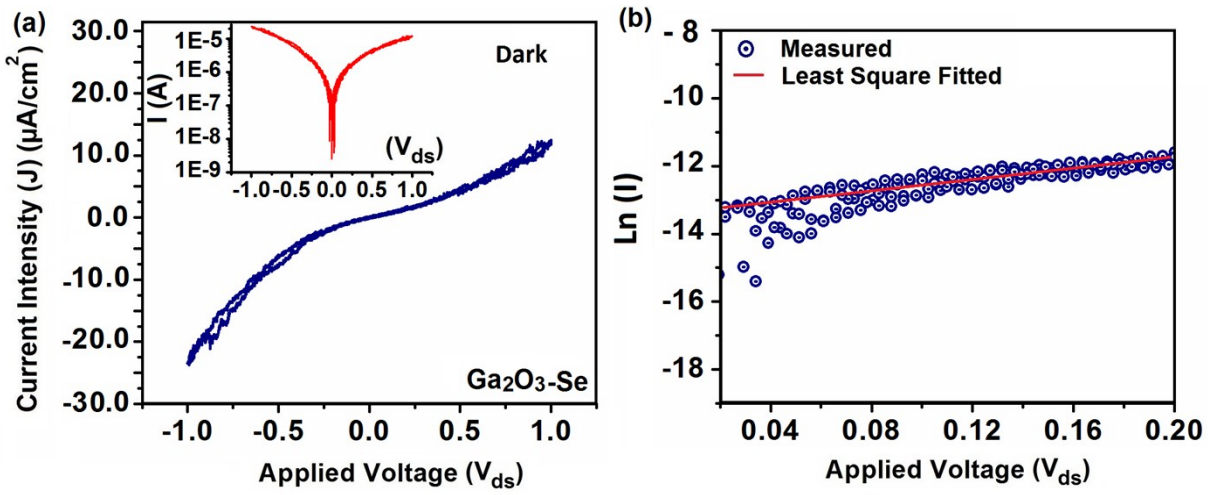

Figure S16. The *J*-V_{ds} characteristics of Au/Ga_2O_3 (Se) nanosheets device and (b) *LnJ*-*V* plot of the Au/Ga_2O_3 (Se) junction (Schottky diode) at the 273K.

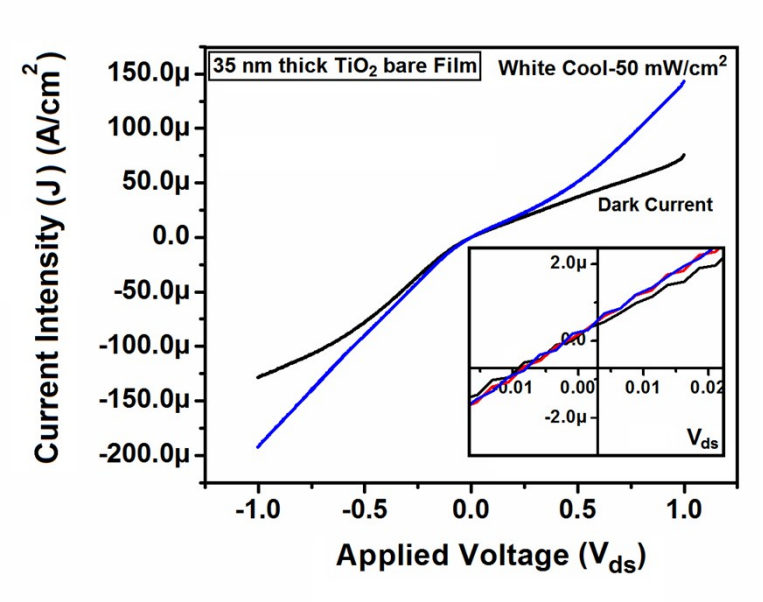

Figure S17. The current intensity versus V_{ds} for TiO_2 photodetectors.

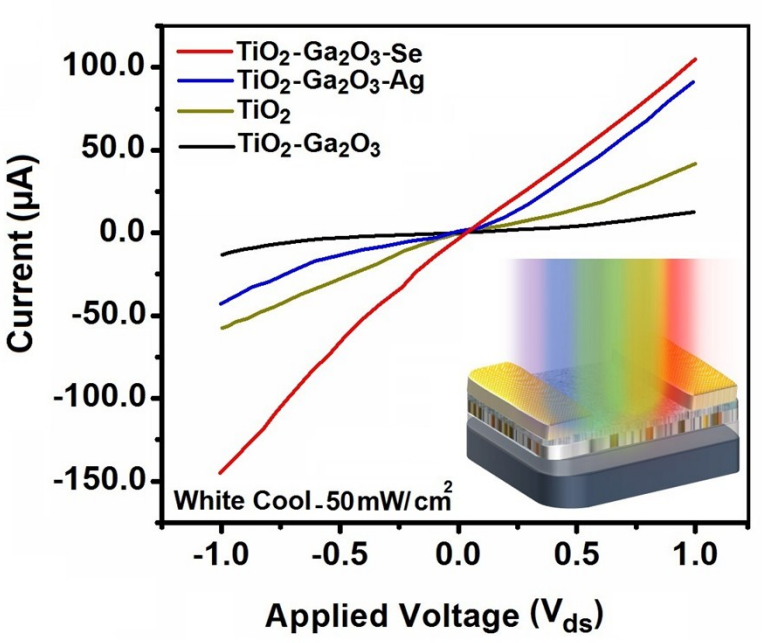

Figure S18. The *I-V* characteristics of Heterostructured PDs.

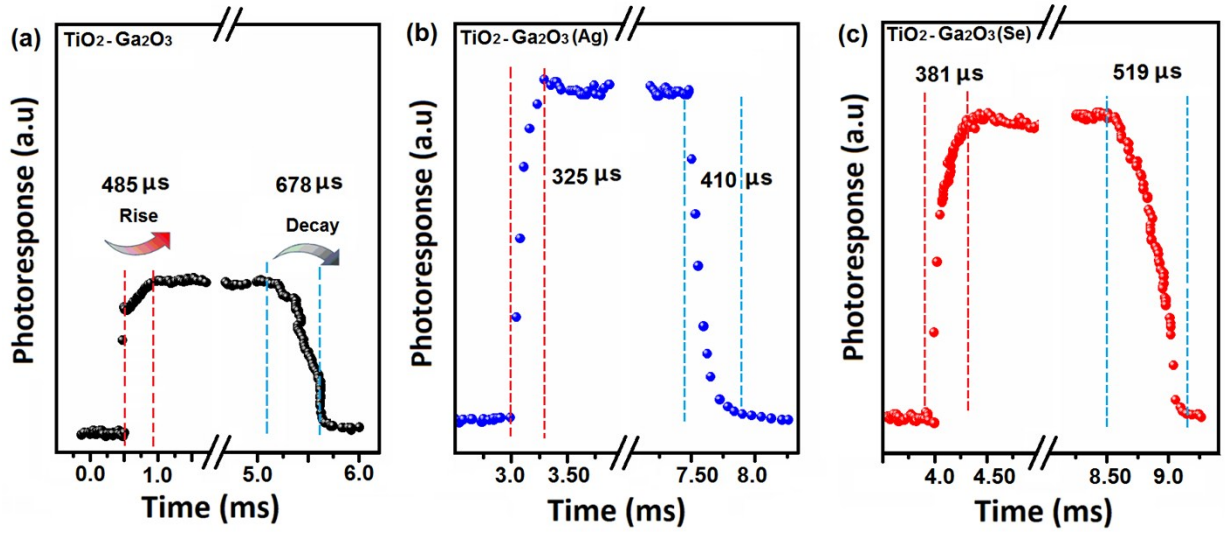

Figure S19. The response and recovery time of heterostructured photodetectors. (a) TiO_2-Ga_2O_3, (b) TiO_2-Ga_2O_3 (Ag), and (c) TiO_2-Ga_2O_3 (Se).

S3- Calculation of IPCE

To calculate IPCE the following formula was used, where the J_{sc} is short circuit current, λ is the wavelength of LED light and P_{IN} is light intensity:

$$IPCE = 1239\left(\frac{j_{sc}}{\lambda.P_{IN}}\right).100$$

(4)

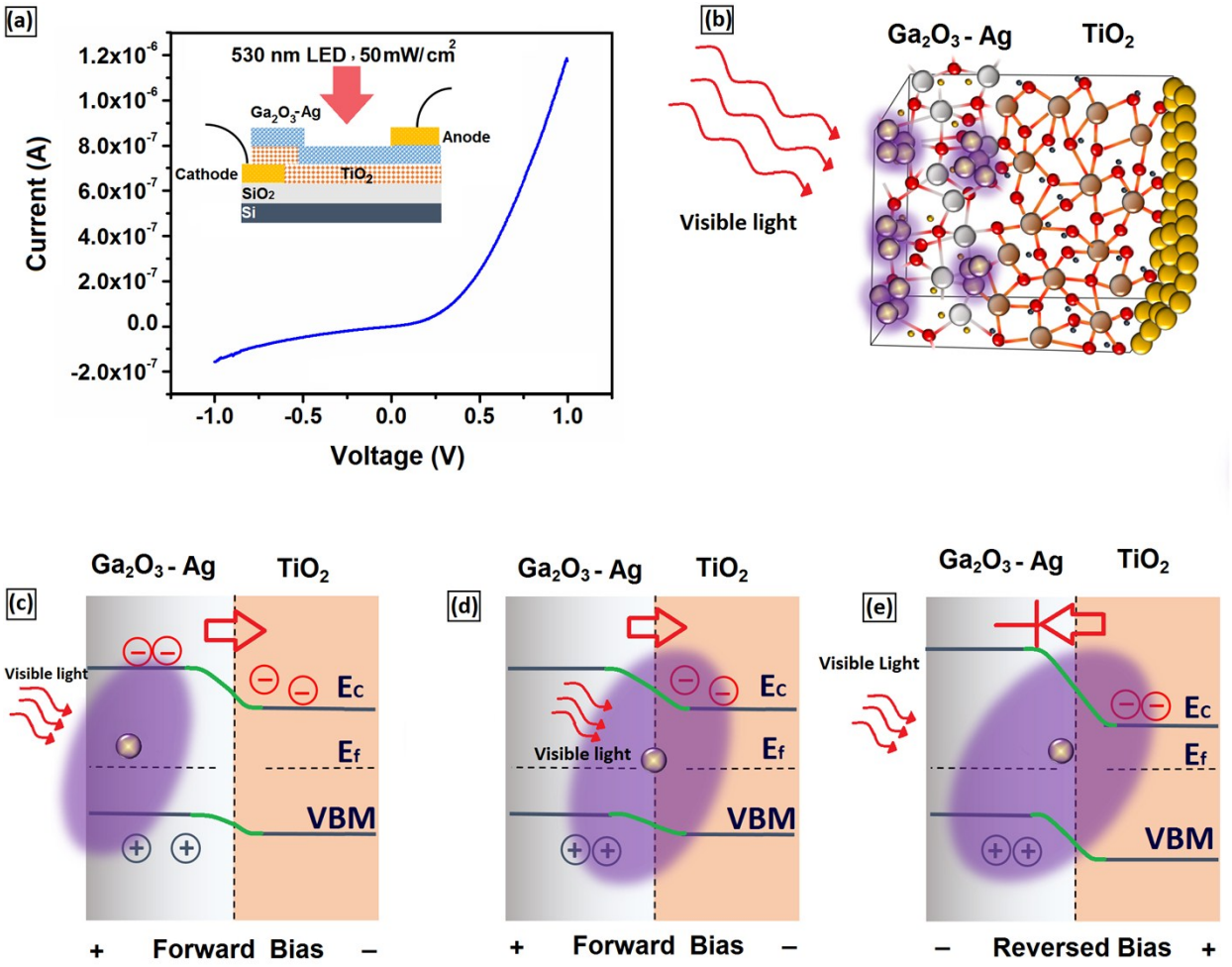

Figure S20. Photoresponse of heterostructure under visible light illumination. (a) The output characteristic (I_{ds}-V_{ds}) of TiO_2-Ga_2O_3 (Ag) heterojunction device under illumination of λ=530 nm LED light (50 mW/cm^2). Top bias electrode is in contact with functionalized Ga_2O_3 nanosheets and cathode electrode is in contact with TiO_2 film which is grounded. (b) Under the illumination of visible light over the heterojunction, most of the carriers are photogenerated in Ga_2O_3 (Ag) part. The proposed mechanism is called Plasmon induced interfacial charge transfer transition in which surface Plasmon (SP) excitation in Ag nanostructures leads to generation of hot

carriers in adjacent semiconductors. In detail, the collective oscillations of electrons in Ag nanostructures generate an intense electric filed with penetration depth of more than 10 nm. In (c) and (d) the so-called hotspot electric filed penetrates into adjacent semiconductor (either Ga_2O_3 or TiO_2), which can excite electron from valence band to conduction band of semiconductor. At the interface of heterojunctions, TiO_2 film depletes electrons at junction, which leads to upward bending and Ga_2O_3 film depletes holes which results in downward bending. Under a forward bias the junction barrier is decreased and the fermi levels of semiconductors are adjusted again. The flowing currents through the heterojunction will increase with the increase of voltage bias. (e) Under a reversed bias voltage, the current cannot overcome the junction barrier and the device maintains the off-set state. The increase of reverse bias voltage facilitates the condition in which the width of junction barrier will severely thinned, consequently the situation for tunneling of carriers is facilitated. By increasing the reversed bias voltage more carries have the opportunity to tunnel into adjacent semiconductor. So the small value of current in reversed bias voltage is the possible consequence of tunneling of carriers from junction barrier in higher revered bias voltage (V_{bs}=-1 V in Figure S20a and its corresponding schematics in Figure S20e).

S4: Band alignment calculation in TiO_2-Ga_2O_3 heterostructure

Based on Kraut's method, the valence band offset (VBO) can be extracted by following formula[4,5]:

$$\Delta E_V = \left(E_{Ga\,2P}^{Ga_2O_3} - E_{VBM}^{Ga_2O_3}\right) - \left(E_{Ti\,2P}^{TiO_2} - E_{VBM}^{TiO_2}\right) - \left(E_{Ga\,2P}^{Ga_2O_3} - E_{Ti\,2P}^{TiO_2}\right) \quad (5)$$

In which $E_{Ga\,2P}^{Ga_2O_3}$ is core level (CL) spectra of Ga 2p, $E_{VBM}^{Ga_2O_3}$ is the valence band maximum (VBM) of Ga_2O_3, $E_{Ti\,2P}^{TiO_2}$ is the CL of Ti 2P spectra, $E_{VBM}^{TiO_2}$ is the VBM of TiO_2. To calculate the VBM of Ga_2O_3 and TiO_2, the XPs spectra of Ga_2O_3 (Ag) and TiO_2 were used (Figure S21).

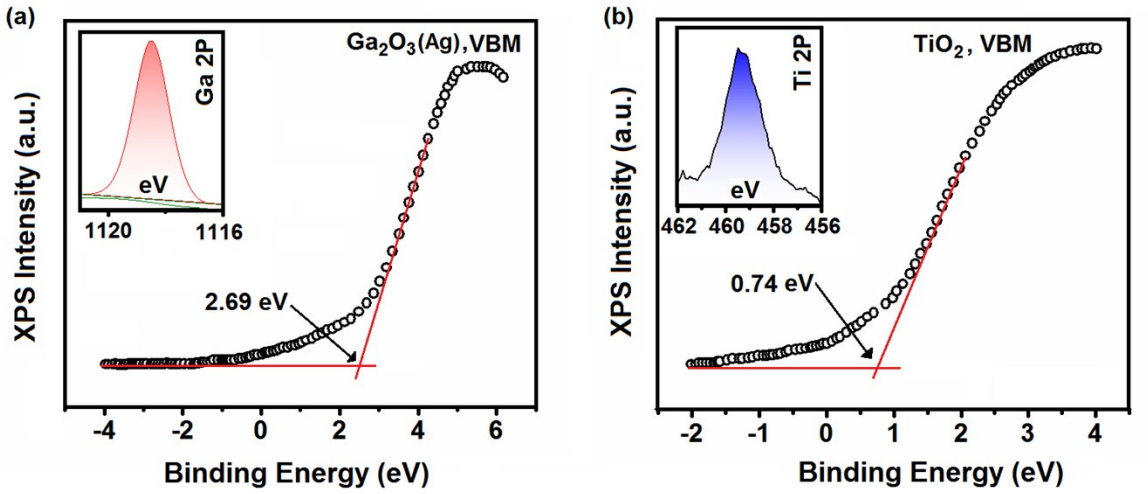

Figure S21. The VBM of the Ga_2O_3 (Ag) and TiO_2 films by extrapolating XPS graphs.

To describe the integrated band offsets of TiO_2-Ga_2O_3 (Ag) heterojunction, the corresponding energy difference between conduction bands can be calculated from Formula (6)[4,5]:

$$\Delta E_C = E_{Bandgap}^{Ga_2O_3} - E_{Bandgap}^{TiO_2} - \Delta E_V \quad (6)$$

Using the above equation and by employment of the XPS spectra of Ga_2O_3 (Ag), TiO_2 and TiO_2-Ga_2O_3 (Ag) heterostructure, the band alignment diagram of TiO_2-Ga_2O_3 (Ag) heterostructure can be calculated. The values of ΔE_V and ΔE_C for the TiO_2-Ga_2O_3 (Ag) heterostructure are respectively -1.95 eV and 3.57 eV. Based on bandgap measurements and band alignment calculation, the simplified band diagram of TiO_2-Ga_2O_3 (Ag) heterostructure is shown in Figure S22, which shows a Type II heterointerfaces.

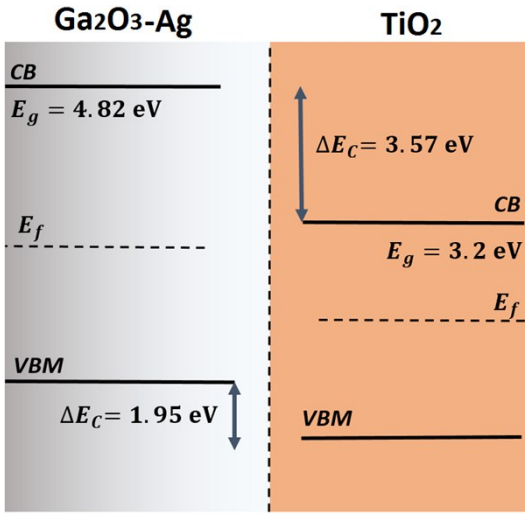

Figure S22. The simplified band alignment diagram for TiO_2-Ga_2O_3 (Ag) heterostructure.

References:

1. S. Gholami, M. Khakbaz, *Int. j. sci. eng.* 2011, **5**, 1285-1288.
2. L. A. M. Lyle, L Jiang, K. K. Das, L. M. Porter. Schottky contact to β-Ga_2O_3. Chapter in: S. Pearton, F. Ren, M. Mastro, Gallium oxide technology, device and applications, 1st ed. Elsevier Science, 2019.
3. K. Sasaki, et al., *IEEE Electron Device Lett*., 2013, **34 (4)**, 493–495.
4. S. M. Sun, W. J. Liu, Y. P. Wang, Y, W. Huan, Q. Ma, B. Zhu, S.D Wu, W.J. Yu, et al., *Appl. Phys. Lett.*, 2018, **113**, 031603.
5. E. A. Kraut, R. W. Grant, J. R. Waldrop, S. P. Kowalczyk, *Phys. Rev. B.* 1983, **28**, 1965-1977.